J|A|C|S ARTICLES

Published on Web 10/08/2010

Visible-Light-Driven Cu(II)−$(Sr_{1-y}Na_y)(Ti_{1-x}Mo_x)O_3$ Photocatalysts Based on Conduction Band Control and Surface Ion Modification

Xiaoqing Qiu,[†] Masahiro Miyauchi,*[,‡] Huogen Yu,[†] Hiroshi Irie,[⊥] and Kazuhito Hashimoto*[,†,§]

Research Center for Advanced Science and Technology, The University of Tokyo, 4-6-1 Komaba, Meguro-ku, Tokyo 153-8904, Japan, National Institute of Advanced Industrial Science and Technology, Tsukuba Central 5, 1-1-1 Higashi, Tsukuba, Ibaraki 305-8565, Japan, Clean Energy Research Center, University of Yamanashi, 4-3-11 Takeda, Kofu, Yamanashi 400-8511, Japan, and Graduate School of Engineering, The University of Tokyo, 7-3-1 Hongo, Bunkyo-ku, Tokyo 113-8656, Japan

Received July 2, 2010; E-mail: m-miyauchi@aist.go.jp; hashimoto@light.t.u-tokyo.ac.jp

Abstract: Band-gap narrowing is generally considered to be a primary method in the design of visible-light-active photocatalysts because it can decrease the photo threshold to lower energies. However, controlling the valence band by up-shifting the top of the band or inducing localized levels above the band results in quantum efficiencies under visible light much lower than those under UV irradiation (such as those reported for N-doped TiO_2: *Science* **2001**, *293*, 269. *J. Phys. Chem. B* **2003**, *107*, 5483). Herein, we report a systematic study on a novel, visible-light-driven photocatalyst based on conduction band control and surface ion modification. Cu(II)−$(Sr_{1-y}Na_y)(Ti_{1-x}Mo_x)O_3$ photocatalysts were prepared by a soft chemical method in combination with an impregnation technique. It is found that Mo^{6+} as well as Na^+ doping in the $SrTiO_3$ can lower the bottom of the conduction band and effectively extend the absorption edge to the visible light region. The Cu(II) clusters grafted on the surface act as a co-catalyst to efficiently reduce the oxygen molecules, thus consuming the excited electrons. Consequently, photocatalytic decomposition of gaseous 2-propanol into CO_2 is achieved, that is, $CH_3CHOHCH_3 + {}^9/_2O_2 \rightarrow 3CO_2 + H_2O$. For Cu(II)−$(Sr_{1-y}Na_y)(Ti_{1-x}Mo_x)O_3$ at $x = 2.0\%$ under visible light irradiation, the maximum CO_2 generation rate can reach 0.148 μmol/h; the quantum efficiency under visible light is calculated to be 14.5%, while it is 10% under UV light irradiation. Our results suggest that high visible light photocatalytic efficiency can be achieved by combining conduction band control and surface ion modification, which provides a new approach for rational design and development of high-performance photocatalysts.

1. Introduction

Considering the current energy and environmental issues at the global level, heterogeneous photocatalysis using semiconductors has a great potential for industrial uses.[1] In general, high performance of photocatalysts requires a high redox potential of photogenerated charge carriers,[2] that is, high oxidation power of the holes in the valence band (VB) and enough reduction power of the electrons in the conduction band (CB). Therefore, the most efficient photocatalysts are usually wide-gap semiconductors, such as TiO_2, ZnO, and $SrTiO_3$. These wide-band-gap semiconductors only show activity under ultraviolet (UV) light irradiation, which limits their practical applications. For effective utilization of solar energy and indoor light, many efforts have been made to develop visible-light-driven photocatalysts.[3] Typically, to tailor the band-gap energies of photocatalysts and extend their absorption to the visible light region, cationic doping with transition metal ions, such as Cr, Mn, Fe, Pb, Cu, and so on, or anionic doping with N, C, and S is commonly used.[4] Even though most photocatalysts doped in this way can exhibit visible light sensitivity, their quantum efficiencies (QEs) under visible light are much lower than those under UV irradiation.[5] In the case of cationic doping, the sensitivity to visible light is mainly due to high levels of impurities in the forbidden band of the photocatalysts, which unfortunately serve as recombination centers for photoinduced

[†] Research Center for Advanced Science and Technology, The University of Tokyo.
[‡] National Institute of Advanced Industrial Science and Technology.
[⊥] Clean Energy Research Center, University of Yamanashi.
[§] Graduate School of Engineering, The University of Tokyo.

(1) (a) Thompson, T. L.; Yates, J. T. *Chem. Rev.* **2006**, *106*, 4428. (b) Kudo, A.; Miseki, Y. *Chem. Soc. Rev.* **2009**, *38*, 253. (c) Hoffmann, M. R.; Martin, S. T.; Choi, W. Y.; Bahnemann, D. W. *Chem. Rev.* **1995**, *95*, 69. (d) Chen, X.; Mao, S. S. *Chem. Rev.* **2007**, *107*, 2891.
(2) Ohtani, B. *Chem. Lett.* **2008**, *37*, 216.
(3) (a) Zou, Z. G.; Ye, J. H.; Sayama, K.; Arakawa, H. *Nature* **2001**, *414*, 625. (b) Rodrigues, S.; Ranjit, K. T.; Uma, S.; Martyanov, I. N.; Klabunde, K. J. *Adv. Mater.* **2005**, *17*, 2467. (c) Maeda, K.; Teramura, K.; Lu, D. L.; Takata, T.; Saito, N.; Inoue, Y.; Domen, K. *Nature* **2006**, *440*, 295. (d) Qiu, X. F.; Zhao, Y. X.; Burda, C. *Adv. Mater.* **2007**, *19*, 3995. (e) Wang, D. F.; Kako, T.; Ye, J. H. *J. Am. Chem. Soc.* **2008**, *130*, 2724. (f) Nakamura, R.; Okamoto, A.; Osawa, H.; Irie, H.; Hashimoto, K. *J. Am. Chem. Soc.* **2007**, *129*, 9596. (g) Weare, W. W.; Pushkar, Y.; Yachandra, V. K.; Frei, H. *J. Am. Chem. Soc.* **2008**, *130*, 11355. (h) Li, G. H.; Dimitrijevic, N. M.; Chen, L.; Rajh, T.; Gray, K. A. *J. Phys. Chem. C* **2008**, *112*, 19040.

charger carries.[1a,6] On the other hand, anionic doping generally contributes to VB control by inducing localized levels above the VB. The holes generated in the localized levels have less oxidation power and mobility than those in the VB, which results in low photocatalytic performance.[5] In fact, oxidative holes in the VB can drive the complete mineralization of organic pollutants, once the photogenerated electrons are efficiently consumed in the presence of oxygen molecules in the air.[2] Therefore, it has significant importance to design photocatalysts that utilize the high oxidation power of holes in the VB under visible light irradiation.

Recently, members of our laboratory designed visible-light-driven photocatalysts by grafting Cu^{2+} ions onto TiO_2 surfaces.[7] Under visible light irradiation, electrons in the VB of TiO_2 can be transferred to Cu(II) clusters, i.e., interfacial charge transfer (IFCT),[8] resulting in the formation of Cu(I) clusters. Cu(I) clusters can efficiently reduce oxygen molecules,[7] thus consuming the excited electrons. The holes generated in the VB can decompose the organic compounds. In other words, this system can take advantage of both the efficient oxygen reduction via Cu ions and the high oxidation power of the holes in the VB of TiO_2 induced by IFCT under visible light irradiation. However, IFCT is an interface phenomenon, and the IFCT absorption is rather weak.[8] It should be noted that tungsten trioxide (WO_3) has the proper band gap for good visible light absorption. Despite the high oxidation power of the holes in the VB, WO_3 was once considered to be inactive because of the low potential of electrons in the CB. Encouragingly, upon modification of WO_3 with co-catalysts such as Pt, Pd, WC, CuO, or Cu(II) clusters, the visible light activity was drastically enhanced via the efficient oxygen reduction process.[9] Previous studies suggested that the photogenerated electrons in WO_3 are injected into these co-catalysts, and these injected electrons cause multielectron reductions to produce active species such as hydrogen peroxides.[9] However, the chemical stability of WO_3 is low, and tungsten is an expensive, rare metal; thus, it is not suitable for industrial applications. These elaborate works give us a hint that CB control might be a good way to enhance visible light absorption, leaving the oxidation power of the holes unchanged. Moreover, combining CB control and efficient oxygen reduction via Cu ions grafted on the photocatalysts' surfaces is a novel approach that is likely to provide an opportunity for designing highly efficient visible-light-driven photocatalysts. We recently demonstrated that CB-controlled TiO_2 co-doped with W^{6+} and Ga^{3+} showed visible light sensitivity after Cu(II) ions were grafted on the surfaces, even though the visible light absorption was rather low.[10]

Bearing these issues in mind, we selected strontium titanate ($SrTiO_3$) as a wide-band-gap semiconductor for our study system, based on the following considerations: (1) $SrTiO_3$, one of the most promising semiconductors, has versatile applications in the electronics industry and photocatalysis due to its merits of thermal and structural stability and resistance to photocorrosion.[11] (2) Most importantly, $SrTiO_3$ has a perovskite cubic structure with the general formula ABO_3, which provides the flexibility to vary the composition of A and B sites to form substituted nonstoichiometric perovskite and tune the electronic structure.[12] Further, the electronic structure of $SrTiO_3$ resembles that of TiO_2, whose valence band is deep, and therefore photogenerated holes can oxidize most organic compounds.[11b] On the basis of our calculations of electronic density of states (DOS), we design conduction-band-controlled $SrTiO_3$ by co-doping. In the present study, we found that Mo^{6+} as well as Na^+ is an optimum dopant for lowering the conduction band level. We synthesized $SrTiO_3$ co-doped with Mo^{6+} and Na^+ by a simple hydrothermal reaction. After Cu(II) modification on the surfaces of doped $SrTiO_3$, the photocatalysts exhibit high activities for oxidation of gaseous 2-propanol (IPA) to CO_2 under visible light irradiation.

2. Experimental Section

2.1. Synthesis of $(Sr_{1-y}Na_y)(Ti_{1-x}Mo_x)O_3$ Samples. The $(Sr_{1-y}Na_y)(Ti_{1-x}Mo_x)O_3$ samples were prepared by a hydrothermal method. $Sr(OH)_2 \cdot 8H_2O$, amorphous TiO_2, and Na_2MoO_4 were used as the starting materials. All chemicals were analytical grade, used without further purification. The synthesis procedure is described as follows: 5.315 g (0.02 mol) of $Sr(OH)_2 \cdot 8H_2O$, 1.597 g (0.02 mol) of amorphous TiO_2, and given amounts of Na_2MoO_4 were added into 80 mL of distilled water to form a white suspension. This suspension was transferred to a 100 mL Teflon-lined, stainless steel autoclave and allowed to react at 140 °C for 20 h. The autoclave was then cooled naturally to room temperature. The products were harvested by pressure filtration with a membrane filter (0.025 μm, Millipore), washed with diluted HCl and distilled water, and dried in air at ambient temperature. To improve the crystallinity, the products were calcined at 600 °C for 10 h. The samples thus obtained were denoted as $(Sr_{1-y}Na_y)(Ti_{1-x}Mo_x)O_3$.

To get the samples with different Na^+ contents and roughly fixed Mo^{6+} content, parallel control experiments were performed under identical conditions.

Control Experiment I: 5.315 g (0.02 mol) of $Sr(OH)_2 \cdot 8H_2O$, 1.597 g (0.02 mol) of amorphous TiO_2, 0.106 g (0.513 mmol) of $NaMoO_4$, and 10 g of NaCl were used as the starting materials.

(4) (a) Asahi, R.; Morikawa, T.; Ohwaki, T.; Aoki, K.; Taga, Y. *Science* **2001**, *293*, 269. (b) Wang, D. F.; Ye, J. H.; Kako, T.; Kimura, T. *J. Phys. Chem. B* **2006**, *110*, 15824. (c) Kudo, A.; Niishiro, R.; Iwase, A.; Kato, H. *Chem. Phys.* **2007**, *339*, 104. (d) Kato, H.; Kudo, A. *J. Phys. Chem. B* **2002**, *106*, 5029. (e) Irie, H.; Maruyama, Y.; Hashimoto, K. *J. Phys. Chem.C* **2007**, *111*, 1847. (f) Xie, T. H.; Sun, X. Y.; Lin, J. *J. Phys. Chem. C* **2008**, *112*, 9753. (g) Miyauchi, M.; Takashio, M.; Tobimatsu, H. *Langmuir* **2004**, *20*, 232. (h) Sun, X. Y.; Lin, J. *J. Phys. Chem. C* **2009**, *113*, 4970. (i) Wang, D. F.; Ye, J. H.; Kako, T.; Kimura, T. *J. Phys. Chem. B* **2006**, *110*, 15824. (j) Mrowetz, M.; Balcerski, W.; Colussi, A. J.; Hoffmann, M. R. *J. Phys. Chem. B* **2004**, *108*, 17269.

(5) Irie, H.; Watanabe, Y.; Hashimoto, K. *J. Phys. Chem. B* **2003**, *107*, 5483.

(6) (a) Konta, R.; Ishii, T.; Kato, H.; Kudo, A. *J. Phys. Chem. B* **2004**, *108*, 8992. (b) Choi, W. Y.; Termin, A.; Hoffmann, M. R. *J. Phys. Chem.* **1994**, *98*, 13669.

(7) (a) Irie, H.; Miura, S.; Kamiya, K.; Hashimoto, K. *Chem. Phys. Lett.* **2008**, *457*, 202. (b) Irie, H.; Kamiya, K.; Shibanuma, T.; Miura, S.; Tryk, D. A.; Yokoyama, T.; Hashimoto, K. *J. Phys. Chem. C* **2009**, *113*, 10761.

(8) (a) Creutz, C.; Brunschwig, B. S.; Suntin, N. *J. Phys. Chem. B* **2005**, *109*, 10251. (b) Creutz, C.; Brunschwig, B. S.; Suntin, N. *J. Phys. Chem. B* **2006**, *110*, 25181. (c) Hush, N. S. *Electrochim. Acta* **1968**, *13*, 1005. (d) Hush, N. S. *J. Electroanal. Chem.* **1999**, *460*, 5. (e) Hush, N. S. *J. Electroanal. Chem.* **1999**, *470*, 170.

(9) (a) Abe, R.; Takami, H.; Murakami, N.; Ohtani, B. *J. Am. Chem. Soc.* **2008**, *130*, 7780. (b) Zhao, Z. G.; Miyauchi, M. *Angew. Chem., Int. Ed.* **2008**, *47*, 7051. (c) Arai, T.; Horiguchi, M.; Yanagida, M.; Gunji, T.; Sugihara, H.; Sayama, K. *Chem. Commun.* **2008**, 5565. (d) Kim, Y. H.; Irie, H.; Hashimoto, K. *Appl. Phys. Lett.* **2008**, *92*, 182107. (e) Arai, T.; Yanagida, M.; Konishi, Y.; Iwasaki, Y.; Sugihara, H.; Sayama, K. *Catal. Commun.* **2008**, *9*, 1254.

(10) Yu, H. G.; Irie, H.; Hashimoto, K. *J. Am. Chem. Soc.* **2010**, *132*, 6898.

(11) (a) Bolts, J. M.; Wrighton, M. S. *J. Phys. Chem.* **1976**, *80*, 2640. (b) Miyauchi, M.; Nakajima, A.; Fujishima, A.; Hashimoto, K.; Watanabe, T. *Chem. Mater.* **2000**, *12*, 3. (c) Konta, R.; Ishii, T.; Kato, H.; Kudo, A. *J. Phys. Chem. B* **2004**, *108*, 8992.

(12) (a) Pena, M. A.; Fierro, J. L. G. *Chem. Rev.* **2001**, *101*, 1981. (b) Chan, N. H.; Sharma, R. K.; Smyth, D. M. *J. Electrochem. Soc.* **1981**, *128*, 1762.

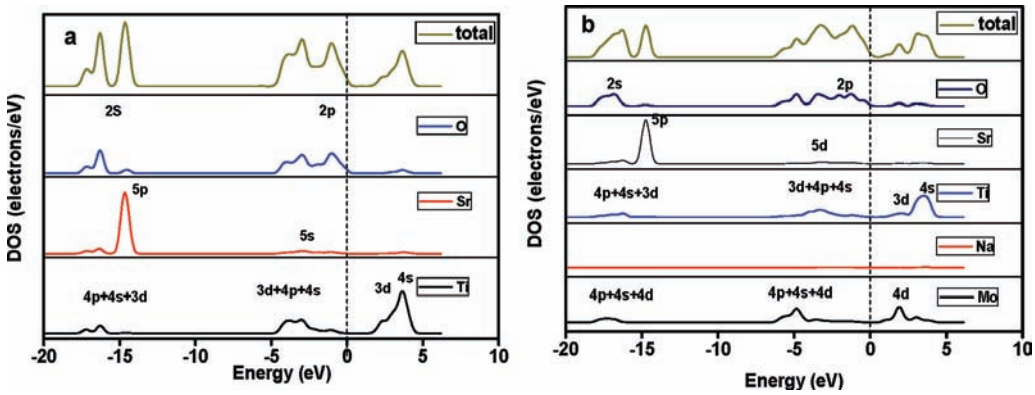

Figure 1. Density of states of (a) $SrTiO_3$ and (b) $(Sr_{1-y}Na_y)(Ti_{1-x}Mo_x)O_3$ (at $x = 0.333$). The vertical dashed line represents the Fermi level.

The remaining procedures were the same as those described above. The sample was named sample V.

Control Experiment II: 5.315 g (0.02 mol) of $Sr(OH)_2 \cdot 8H_2O$, 1.597 g (0.02 mol) of amorphous TiO_2, and 0.074 g (0.513 mmol) of MoO_3 instead of $NaMoO_4$ were used as the starting materials. The remaining procedures were the same as those described above. The sample was named sample VI.

2.2. Modification of $(Sr_{1-y}Na_y)(Ti_{1-x}Mo_x)O_3$ Samples with Cu(II) Ions. The Cu(II)−$(Sr_{1-y}Na_y)(Ti_{1-x}Mo_x)O_3$ photocatalysts were prepared by an impregnation technique that was described in detail in our previous work.[7] In a typical preparation, 1 g of $(Sr_{1-y}Na_y)(Ti_{1-x}Mo_x)O_3$ sample was dispersed into 10 mL of $CuCl_2$ solution in a vial reactor. The weight fraction of Cu^{2+} relative to $(Sr_{1-y}Na_y)(Ti_{1-x}Mo_x)O$ was set to be 1×10^{-3}. Under stirring, the sealed vial reactor was heated at 90 °C for 1 h using a water bath. The suspension was then filtered and washed with a sufficient amount of distilled water. The final products were dried at 110 °C for 24 h and subsequently ground into a powder using an agate mortar.

2.3. Sample Characterization. Elemental analyses of the samples were performed using an inductively coupled plasma atomic emission spectrometer (ICP-AES, P-4010, Hitachi) for Ti, Sr, Mo, and Cu and a polarized Zeeman atomic absorption spectrophotometer (Z-2000, Hitachi) for Na. The structural characteristics of the samples were measured by powder X-ray diffraction (XRD) at room temperature on a Rigaku D/MAX25000 diffractometer with a copper target ($\lambda = 1.54178$ Å). Ni powder served as an internal standard for peak position determination. The data were collected from $2\theta = 20$ to 70° in a step-scan mode (step, 0.02°; counting time, 5 s). The morphologies of the samples were investigated by field-emission scanning electron microscopy (SEM) using a JEOL JSM-6700 apparatus and transition electron microscopy (TEM) on a JEOL JEM 2010 instrument under an acceleration voltage of 200 kV. The specific surface areas of the samples were determined from the nitrogen absorption data at liquid nitrogen temperature using the Barrett−Emmett−Teller (BET) technique. The samples were degassed at 200 °C and a pressure below 100 mTorr for a minimum of 2 h prior to analysis using a Micromeritics VacPrep 061 instrument. The absorption spectra of the samples were recorded using a UV-2550 spectrophotometer (Shimadzu). The ionic characteristics and surface composition were studied by X-ray photoelectron spectroscopy (XPS; Perkin-Elmer model 5600). The binding energy data are calibrated with the C 1s signal at 284.6 eV.

2.4. Evaluation of Photocatalytic Properties. The decomposition of gaseous IPA was chosen as a probe to evaluate the photocatalytic activities of the samples in air. A 500 mL cylindrical glass vessel was used as the photocatalysis reactor. The experiments were carried out according to the following procedure: 300 mg of photocatalyst powder was evenly spread on the bottom of a circular glass dish with an area of 5.5 cm^2, which was mounted in the middle of the vessel reactor. The vessel was sealed with a rubber O-ring and a quartz cover, evacuated, and filled with fresh synthetic air. To eliminate the sample surface organic contaminants, the vessel was pre-illuminated with a Xe lamp (Luminar Ace 210, Hayashi Tokei Works) until the rate of CO_2 generation was less than 0.02 μmol/day. The vessel was re-evacuated and refilled with fresh synthetic air. The pressure inside the vessel was kept at about 1 atm. Next, 300 ppm of gaseous IPA was injected into the vessel. Prior to light irradiation, the vessel was kept in the dark for a sufficient time to ensure the establishment of absorption/desorption equilibrium of IPA on the surfaces of the photocatalysts. Subsequently, the vessel was irradiated under a Xe lamp. A combination of glass filters (B-47, L-42, and C-40C, AGC Techno Glass) was used to obtain visible light with wavelength from 400 to 530 nm. The light intensity was determined by a spectroradiometer (USR-40D, Ushio) and set to be 1 mW/cm^2. To fully understand the photocatalytic performance of the samples, a parallel experiment was conducted under UV light (310−400 nm) irradiation, which is obtained by using a D-36 glass filter. The UV light intensity was adjusted by controlling the absorption photon number of the catalysts to be the same as that under visible light irradiation. During the light irradiation, 1 mL of gaseous sample was periodically extracted from the reaction vessel to monitor the concentrations of IPA, acetone, and CO_2 using a gas chromatograph (model GC-8A, Shimadzu Co., Ltd.).

2.5. Calculations of the Electronic Band Structure. The electronic structure of the samples was calculated using plane-wave-based density functional theory with the CASTEP program package. The ionic cores of the elements were represented by scalar relativistic, fully separable, ultrasoft pseudopotentials. The generalized gradient approximation (GGA-PBE) was applied, and the kinetic energy cutoff was selected at 370 eV. The density of the Monkhorst−Pack k-point mesh was $5 \times 5 \times 3$. The Sr ions and Ti ions were partly substituted by Na^+ ions and Mo^{6+} ions in the $SrTiO_3$ cell to simulate the $(Sr_{1-y}Na_y)(Ti_{1-x}Mo_x)O_3$ system. The compositions used for the calculation were $SrTiO_3$ and $(Sr_{1-y}Na_y)(Ti_{1-x}Mo_x)O_3$ at $x = 0.333$. The system structures were optimized by first-principles calculations.

3. Results and Discussion

The electronic structures of $SrTiO_3$ and $SrTiO_3$ co-doped with Mo^{6+} as well as Na^+ were investigated on the basis of the plane-wave density function theory program package CASTEP. The variations of DOS of $SrTiO_3$ with energy are shown in Figure 1a. Zero energy corresponds to the Fermi level (E_F). The VB of $SrTiO_3$ consists of O 2p, Sr 5s, and Ti 3d hybrid orbitals; the O 2p is closer to E_F and contributes more electrons, while the bottom of the CB above E_F is predominantly composed of Ti 3d-like states. To understand the qualitative impact of Na^+ and Mo^{6+} co-doping on the DOS, the unit cells of $(Sr_{1-2y}Na_y)(Ti_{1-x}Mo_x)O_3$ were constructed by partially substitut-

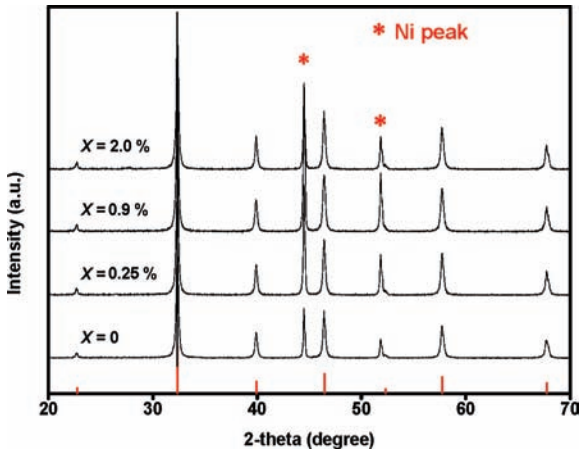

Figure 2. XRD patterns of $(Sr_{1-y}Na_y)(Ti_{1-x}Mo_x)O_3$ at $x = 0$, 0.25, 0.9, and 2.0%. Vertical bars below the patterns represent the standard diffraction data from the JCPDS file for bulk $SrTiO_3$ (No. 86-0176). Peaks marked with an asterisk are due to the internal standard nickel.

ing Na^+ ions at the Sr^{2+} lattice site and Mo^{6+} ions at the Ti^{4+} site in cubic perovskite $SrTiO_3$. As illustrated in Figure 1b, Mo 4d-like states are located below the Ti 3d orbital and contribute to the bottom of the CB, resulting in the band narrowing. However, the VB remains almost the same as that of non-doped $SrTiO_3$. Na^+ ions do not directly contribute to the energy structure but construct the crystal structures.[1b] The theoretical calculations demonstrate that Mo^{6+} and Na^+ are optimum dopants for lowering the CB level.

Elemental analyses of the samples were performed using ICP-AES for Ti, Sr, Mo, and Cu and a polarized Zeeman atomic absorption spectrophotometer for Na. The results are listed in Table S1 (Supporting Information). The Mo contents in the samples were close to the initial ones in hydrothermal solution. Although relatively small amounts of Na were also detected in the doped samples, we could synthesize $SrTiO_3$ co-doped with Mo and Na by a simple hydrothermal method. The relatively low amount of Na is partly because of the high solubility of Na in the aqueous solution under hydrothermal conditions. For all the as-obtained samples, the Ti content was slightly higher than the Sr content. Hereafter, Mo- and Na-doped $SrTiO_3$ is described as $(Sr_{1-y}Na_y)(Ti_{1-x}Mo_x)O_3$.

Figure 2 shows the XRD patterns of $(Sr_{1-y}Na_y)(Ti_{1-x}Mo_x)O_3$ samples that were obtained by the hydrothermal method with heat treatment at 600 °C for 10 h. With varying Mo content $x \leq 2.0\%$, the peak position matched well the standard data for bulk $SrTiO_3$ (JCPDS card No. 86-0176). Therefore, all the samples crystallized in a cubic perovskite structure with high crystallinity, as indicated by the sharp XRD peaks. No peaks associated with rutile or anatase TiO_2, MoO_3, or $SrMoO_4$ were detected. From the enlarged (110) peaks (Figure S1, Supporting Information), there was no obvious shift of peak position with varying contents of Mo^{6+} and Na^+. It is well known that $SrTiO_3$ is a typical ABO_3 perovskite material in which the A site may accommodate alkaline-earth, alkali, and rare-earth cations. Fujimoto et al.[13] demonstrated that Na^+ ions substituted for Sr^{2+} rather than Ti^{4+} in $SrTiO_3$ because the 12-coordinated effective radius of Na^+ ions (1.39 Å) is very close to that of Sr^{2+} (1.44 Å).[14] Devi and Murthy[15] found that Mo^{6+} ions were prone to replace Ti^{4+} due to the good ionic radius matching between Mo^{6+} (0.62 Å) and Ti^{4+} (0.605 Å) in six-fold coordination. Therefore, for our study, Na^+ ions are more likely to be introduced into the A site and Mo^{6+} ions into the B site of $SrTiO_3$ to form the compound $(Sr_{1-y}Na_y)(Ti_{1-x}Mo_x)O_3$. The preliminary observations imply that the perovskite structure is not disturbed by the addition of small amounts of Mo^{6+} and Na^+ during the sample preparation procedure, and the incorporation of Mo^{6+} and Na^+ induces no significant change in the lattice size, due to the similarities in the ions radii. When the Mo content was further increased to $x = 5\%$, several additional peaks assigned to the secondary phase of $SrMoO_4$ appeared (Figure S2, Supporting Information). Because of the detection limitation of XRD measurements, the structure of the samples was further investigated using SEM, TEM, XPS, and UV−visible spectroscopy.

Morphologies of the $(Sr_{1-y}Na_y)(Ti_{1-x}Mo_x)O_3$ samples were observed by SEM. As can be seen in Figure 3, all the samples were an assembly of uniformly distributed nanoparticles. The average grain size of the nanoparticles was about 50 nm. Introduction of a small amount of Mo^{6+} as well as Na^+ into the $SrTiO_3$ lattice did not change the morphology or the particle size. Therefore, the effects of morphology and size on the photocatalytic activity[16] can be excluded in the present study. A TEM image of non-doped $SrTiO_3$ (at $x = 0$) further showed that the sample consists of particle-like structures (Figure S3, Supporting Information). The corresponding high-resolution TEM image shows clear lattice fringes, demonstrating the single-crystalline nature of these nanoparticles and the high quality of the as-obtained samples. The shape and size of the samples were not disturbed by surface modification with Cu(II) either, as shown in Figure S3. Cu(II) clusters were hardly detected on the sample surfaces by TEM observation, probably because the amount of Cu(II) was extremely low and the Cu(II) clusters are most likely to exist as an amorphous form due to the relatively low grafting temperature,[7a] in contrast to noble metal deposition on the surface of photocatalysts.[9a]

The surface compositions and element chemical states of the samples were investigated by XPS. Figure S4 (Supporting Information) gives a series of full-scale XPS spectra of non-doped $SrTiO_3$, $(Sr_{1-y}Na_y)(Ti_{1-x}Mo_x)O_3$ at $x = 2.0\%$, and Cu(II)−$(Sr_{1-y}Na_y)(Ti_{1-x}Mo_x)O_3$ at $x = 2.0\%$. For the non-doped $SrTiO_3$, only Sr, Ti, and O were detected. Moreover, the spectrum of $(Sr_{1-y}Na_y)(Ti_{1-x}Mo_x)O_3$ at $x = 2.0\%$ clearly showed the additional peaks associated with Mo, while the diagnostic peak of Na overlapped with that of Ti auger. For the Cu(II)−$(Sr_{1-y}Na_y)(Ti_{1-x}Mo_x)O_3$ at $x = 2.0\%$, the signal of Cu was clearly observed, evidencing that Cu(II) was successfully grafted on the surfaces. Figure 4a shows the Mo 3d core-level XPS spectra. The Mo 3d signals increased with the content of Mo in the samples. It is clear that the Mo 3d spectra consist of well-defined photoelectron signals located at 235.6 and 232.5 eV, which can be assigned to Mo $3d_{3/2}$ and Mo $3d_{5/2}$ spin−orbital components, respectively.[17] One can safely conclude that molybdenum in all the samples is present in one oxidation state (Mo^{6+}), consistent with the literature reports.[17] The Ti 2p core-level spectra showed two well-resolved Ti $2p_{1/2}$ and Ti $2p_{3/2}$ spectral lines at 463.9 and 458.2 eV (Figure 4b), in agreement with literature values for Ti^{4+}.[18] No shoulders associated with

(13) Fujimoto, M.; Chiang, Y. M.; Roshko, A.; kingery, W. D. *J. Am. Ceram. Soc.* **1985**, *68*, C300.
(14) Shannon, R. D. *Acta Crystallogr., Sect. A: Cryst. Phys., Diffr., Theor. Gen. Crystallogr.* **1976**, *32*, 751.
(15) Devi, L. G.; Murthy, B. N. *Catal. Lett.* **2008**, *125*, 320.
(16) (a) Wang, H. H.; Xie, C. S.; Zhang, W.; Cai, S. Z.; Yang, Z. H.; Gui, Y. H. *J. Hazard. Mater.* **2007**, *14*, 645. (b) Li, D.; Haneda, H. *Chemosphere* **2003**, *51*, 129.

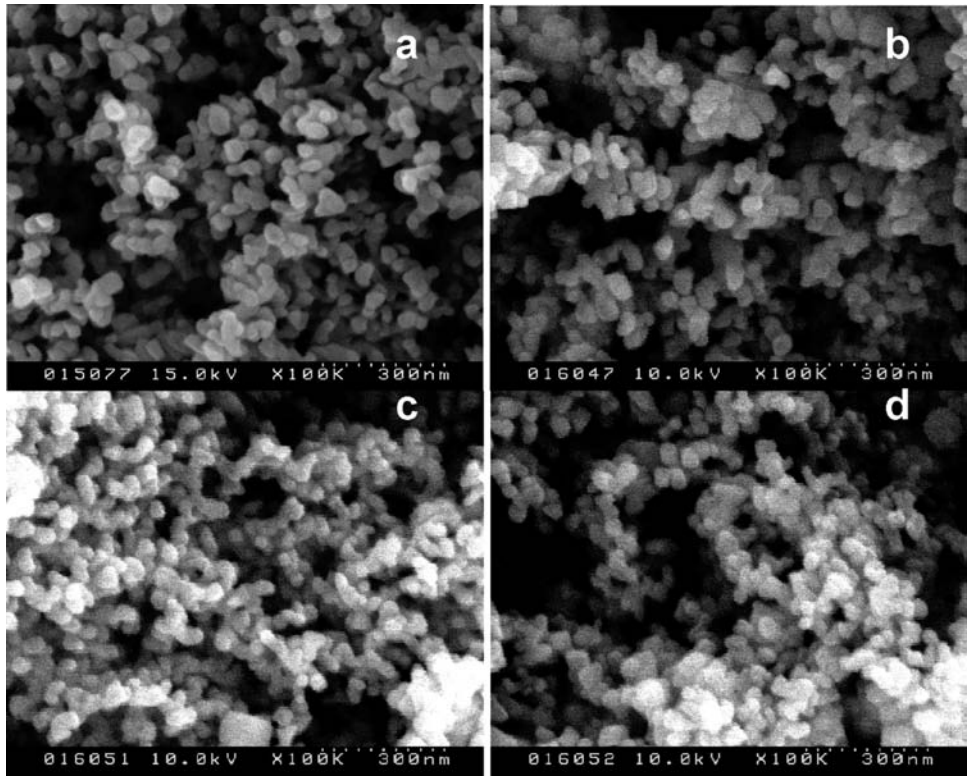

Figure 3. SEM images of $(Sr_{1-y}Na_y)(Ti_{1-x}Mo_x)O_3$ at (a) $x = 0$, (b) $x = 0.25\%$, (c) $x = 0.9\%$, and (d) $x = 2.0\%$.

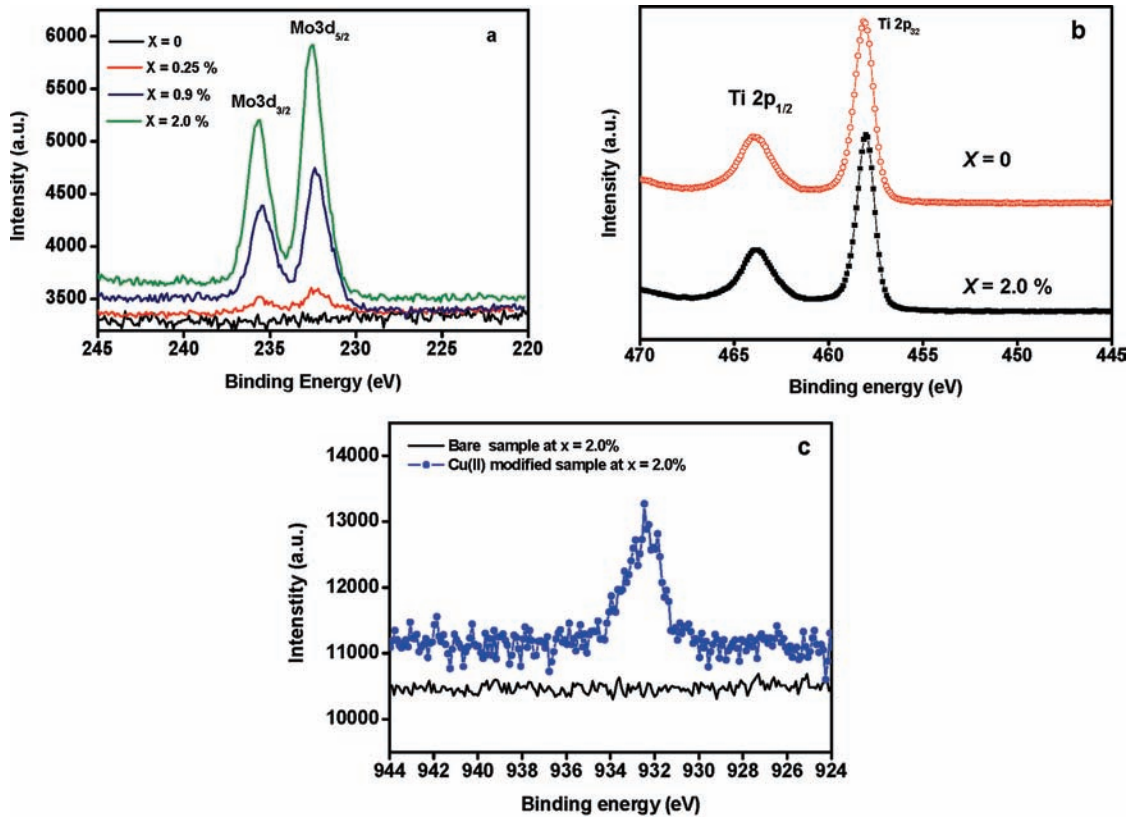

Figure 4. (a) Mo 3d core-level spectra of $(Sr_{1-y}Na_y)(Ti_{1-x}Mo_x)O_3$ samples at $x = 0$, 0.25, 0.9, and 2.0%. (b) Ti 2p core-level spectra of $(Sr_{1-y}Na_y)(Ti_{1-x}Mo_x)O_3$ samples at $x = 0$ and 2.0%. (c) Cu 2p core-level spectra of bare and Cu(II)-modified $(Sr_{1-y}Na_y)(Ti_{1-x}Mo_x)O_3$ samples at $x = 2.0\%$.

Ti^{3+} or Ti^{2+} was observed at the lower energy side. When the Mo content was roughly fixed and the Na content in the samples varied, no obvious differences were seen in the chemical states of Mo and Ti in the samples (Figure S5, Supporting Information). Hitosugi et al. studied the microstructure of Nb^{5+}-doped anatase TiO_2 using XPS and found that the incorporation of

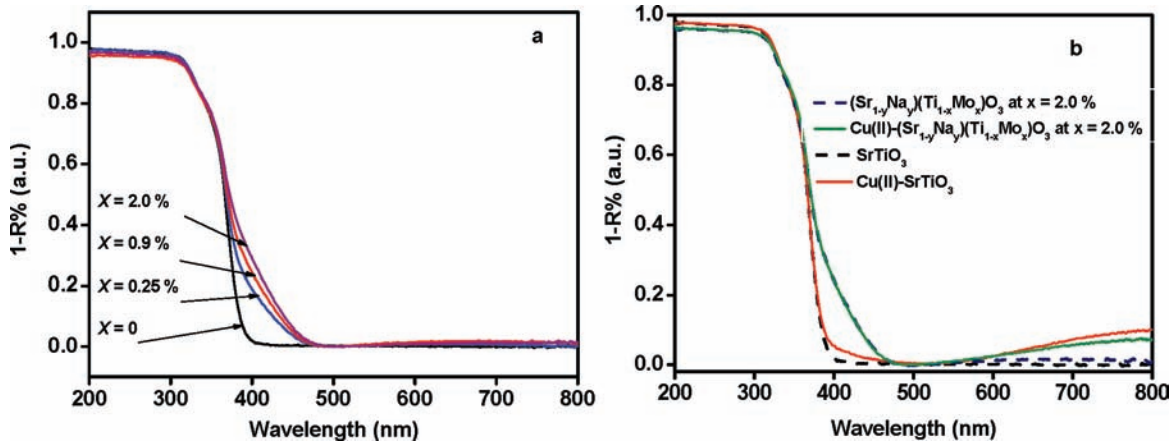

Figure 5. UV−visible absorption spectra of samples. (a) $(Sr_{1-y}Na_y)(Ti_{1-x}Mo_x)O_3$ at $x = 0$, 0.25, 0.9, and 2.0%. (b) Cu(II)−$(Sr_{1-y}Na_y)(Ti_{1-x}Mo_x)O_3$ at $x =$ 0 and 2.0%. The dashed curves correspond to those of the bare samples.

Nb^{5+} into the lattice of TiO_2 resulted in the formation of minor components of Ti^{3+} to keep the charge balance.[19] However, for our study, Mo^{6+} as well as Na^+ doping induced negligible change of the Ti 2p spectrum. Due to the good ionic radius matching between Mo^{6+} and Ti^{4+} in six-fold coordination, Mo^{6+} ions are prone to replace Ti^{4+} of $SrTiO_3$.[15] Besides the ionic radius matching, electroneutrality is another factor to be fulfilled for an ABO_3 perovskite. The important characteristic of ABO_3 perovskites is their susceptibility to partial substitution of cations or deficiencies of cations at both A and B sites.[12] It is well documented that a strontium vacancy is a favorable point defect in $SrTiO_3$,[12,20] especially when Ti/Sr > 1.[12b] According to the above elemental analysis, Sr content was slight lower than that of Ti, which suggests that, in addition to the small amount of Na^+ substituted in A sites,[13] Sr vacancies could play an important role in keeping the charge balance. After modification with Cu(II), the Cu $2p_{3/2}$ core-level XPS signal was evidently observed at 932.3 eV (Figure 4c), which is consistent with the results from our previous analysis.[7b] In our previous work on the Cu(II)−TiO_2 system, details of the Cu(II) state were investigated by the combination of X-ray absorption fine structure (XAFS) measurements and XPS. It was found that Cu(II) was grafted on the surfaces in a distorted, amorphous CuO-like structure with a five-coordinated square pyramidal form. By analogy with the previous study, the chemical state and environment of Cu(II) in the Cu(II)−$(Sr_{1-y}Na_y)(Ti_{1-x}Mo_x)O_3$ samples might be described in the same way. Furthermore, the amount of Cu was determined to be 0.099 wt % by the ICP measurement, nearly equal to the starting ratios used in the preparation.

The optical absorbance properties of $(Sr_{1-y}Na_y)(Ti_{1-x}Mo_x)O_3$ samples, as measured by diffuse reflectance spectroscopy at room temperature, are displayed in Figure 5a. Non-doped $SrTiO_3$ (at $x = 0$) shows the intense interband absorption in the UV region. It should be noted that doping of Mo^{6+} as well as Na^+ narrows the band gap of $SrTiO_3$ and that the absorption edges shift toward a longer wavelength region with increasing content of Mo^{6+}. While the Mo^{6+} content is roughly fixed, the Na^+ content has no obvious effect on the optical absorbance properties (Figure S6a, Supporting Information). From the DOS calculations, it can be concluded that the band gap narrowing is derived from the lowering of the bottom of the CB while the potential of the top of the VB is maintained. Compared with that of $SrTiO_3$, the decrease of the CB bottom levels of $(Sr_{1-y}Na_y)(Ti_{1-x}Mo_x)O_3$ samples at $x = 2.0\%$ was approximately 0.7 eV, estimated from the change in the optical band-gap energies (Figure S6b, Supporting Information). After surface modification with Cu(II), the Cu(II)−$SrTiO_3$ exhibited two additional absorption bands in the range of 800−600 and 460−400 nm, as shown in Figure 5b. The absorption in the range of 800−600 nm is attributed to Cu(II) d−d transition.[21] The weak absorption band at 460−400 nm can be ascribed to IFCT from the VB to Cu(II).[7a] For Cu(II)−$(Sr_{1-y}Na_y)$-$(Ti_{1-x}Mo_x)O_3$ at $x = 2.0\%$, only the additional Cu(II) d−d transition was observed. The IFCT band is masked by the interband transition, due to the narrower band gap of $(Sr_{1-y}Na_y)(Ti_{1-x}Mo_x)O_3$ samples at $x = 2.0\%$. This optical property is expected to find important application in photocatalysis, since more visible light energy might be effectively used by combination of IFCT and band-gap narrowing.

Photocatalytic properties of the samples were evaluated by the decomposition of IPA in air under visible light irradiation. The wavelength of the visible light source was 400−530 nm, and the light intensity was 1 mW/cm^2 (Figure S7, Supporting Information). A typical change in the gas concentration during the decomposition of IPA over Cu(II)−$(Sr_{1-y}Na_y)(Ti_{1-x}Mo_x)O_3$ at $x = 2.0\%$ under visible light irradiation is given in Figure 6a. Prior to light irradiation, almost all of the IPA was adsorbed onto the surfaces of the photocatalysts. With the onset of visible light irradiation, the amount of acetone increased rapidly. After the sharp increase, the acetone concentration started to decrease. Meanwhile, the amount of CO_2 initially increased slowly. Accompanying the decease of acetone, the concentration of CO_2 began to increase quickly. In the later period, the rate of CO_2 generation became slower. The experimental observation is

(17) (a) Choi, J. G.; Thompson, L. T. *Appl. Surf. Sci.* **1996**, *93*, 143. (b) Decanio, S. J.; Cataldo, M. C.; Decanio, E. C.; Storm, D. A. *J. Catal.* **1989**, *119*, 256. (c) Grünert, W.; Stakheev, A. Y.; Mörke, W.; Feldhaus, R.; Anders, K.; Shpiro, E. S.; Minachev, K. M. *J. Catal.* **1992**, *135*, 269.

(18) Oku, M.; Wagatsuma, K.; Kohiki, S. *Phys. Chem. Chem. Phys.* **1999**, *1*, 5327.

(19) Hitosugi, T.; Kamisaka, H.; Yamashita, K.; Nogawa, H.; Furubayashi, Y.; Nakao, S.; Yamada, N.; Chikamatsu, A.; Kumigashira, H.; Oshima, M.; Hirose, Y.; Shimada, T.; Hasegawa, T. *Appl. Phys. Express* **2008**, *1*, 111203.

(20) (a) Tanaka, T.; Matsunaga, K.; Ikuhara, Y.; Yamamoto, T. *Phys. Rev. B* **2003**, *68*, 205213. (b) Mizoguchi, T.; Sato, Y.; Buban, J. P.; Matsunaga, K.; Yamamoto, T.; Ikuhara, Y. *Appl. Phys. Lett.* **2005**, *87*, 241920.

(21) Filho, N. L. D. *Mikrochim. Acta* **1999**, *130*, 233.

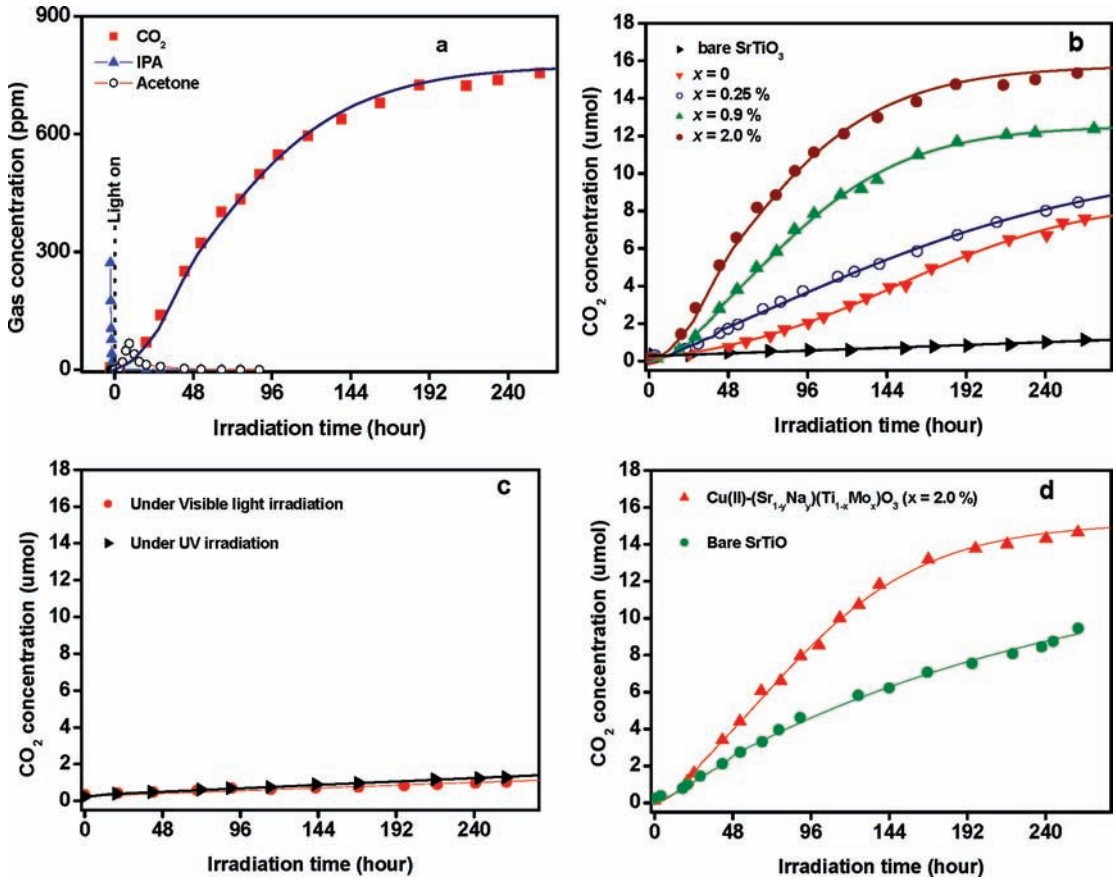

Figure 6. (a) Representative time-dependent gas concentrations during IPA decomposition over Cu(II)−(Sr$_{1-y}$Na$_y$)(Ti$_{1-x}$Mo$_x$)O$_3$ at $x = 2.0\%$ under visible light irradiation. (b) Comparative studies of CO_2 generation over Cu(II)−(Sr$_{1-y}$Na$_y$)(Ti$_{1-x}$Mo$_x$)O$_3$ samples with various Mo contents and bare $SrTiO_3$ under visible light irradiation with the same initial photon flux. (c) Photocatalytic activities of (Sr$_{1-y}$Na$_y$)(Ti$_{1-x}$Mo$_x$)O$_3$ at $x = 2.0\%$ without Cu(II) co-catalyst under visible light and UV irradiation. (d) Photocatalytic activities of Cu(II)−(Sr$_{1-y}$Na$_y$)(Ti$_{1-x}$Mo$_x$)O$_3$ at $x = 2.0\%$ and bare $SrTiO_3$ under UV light irradiation. As for the Figure 6c,d, the UV light intensity was calibrated to keep the absorbed photon numbers the same as that under visible light irradiation.

reasonable, as it is well known that the photocatalytic decomposition of IPA proceeds via formation of acetone as an intermediate, followed by further decomposition of acetone to the final products CO_2 and H_2O.[22] After 260 h of irradiation, the concentration of CO_2 was approximately 900 ppm (ca. ∼18 μmol), which is nearly 3 times the amount of initially injected IPA (300 ppm), indicating the complete decomposition of IPA ($CH_3CHOHCH_3 + {}^9/_2O_2 \rightarrow 3CO_2 + 4H_2O$). Comparative studies of photocatalytic activities of the photocatalysts with various Mo contents under the same visible light source are shown in Figure 6b. CO_2 generation over bare $SrTiO_3$ was negligible because it cannot absorb visible light. In contrast, the Cu(II)-modified, non-doped $SrTiO_3$ (at $x = 0$) was active under visible light, owing to IFCT from the VB of non-doped $SrTiO_3$ to the Cu(II) ions, but its visible light activity was relatively low. More interestingly, the visible light activity of Cu(II)−(Sr$_{1-y}$Na$_y$)(Ti$_{1-x}$Mo$_x$)O$_3$ samples increased with the Mo^{6+} doping up to $x = 2.0\%$, since the visible light absorption increased, as shown in our UV−visible spectra. When the Mo^{6+} doping content was increased to more than 2.0%, the visible light activity of the sample decreased, owing to the formation of inactive $SrMoO_4$ as an impurity.[23] Furthermore, we also optimized the doping density of Na^+ by using NaCl as an additional Na^+ source (sample V) or MoO_3 as the dopant instead of $NaMoO_3$ in our hydrothermal conditions (sample VI). The optimum doping density of Na^+ was less than that expected on the basis of theoretical calculations, probably due to the creation of Sr^{2+} vacancies. Our $SrTiO_3$ sample co-doped with Mo^{6+} as well as Na^+ exhibits better activity than $SrTiO_3$ doped with Mo^{6+} alone (sample VI), but the activity decreased with further increasing the Na^+ content in the sample. One possible reason for this is that Na ions are favored for co-doping in $SrTiO_3$, which does not improve the photocatalytic activity.[24] In the present study, optimum doping densities for Mo^{6+} and Na^+ were 2.0% and 0.25%, respectively (see details in the Supporting Information, Figure S8). On the basis of Figure 6b, the QE for CO_2 generation was calculated using the following equation: $QE = R_p^r/R_p^a = 6R_{CO_2}/R_p^a$, where R_p^r is the reaction rate of photons involved in CO_2 generation, R_{CO_2} is the CO_2 generation rate, and R_p^a is the absorption rate of incident photons. The details for this calculation are described in the literature[7a22] and in the Supporting Information (Figure S9). Some calculated results are summarized in Table 1. Under the same irradiation conditions, the absorption rate of incident photons and the CO_2 generation rate increased as Mo^{6+} content increased. For the Cu(II)−(Sr$_{1-y}$Na$_y$)(Ti$_{1-x}$Mo$_x$)O$_3$ at $x = 2.0\%$, the CO_2 generation rate

(22) Ohko, Y.; Hashimoto, K.; Fujishima, A. *J. Phys. Chem. A* **1997**, *101*, 8057.
(23) Bi, J. H.; Wu, L.; Zhang, Y. F.; Li, Z. H.; Li, J. Q.; Fu, X. Z. *Appl. Catal., B* **2009**, *91*, 135.
(24) (a) Fernandez, A.; Lassaletta, G.; Jimenez, V. M.; Justo, A.; Gonazalez-Elipe, A. R.; Herrmann, J. M.; Tahiri, H.; Ait-Ichou, Y. *Appl. Catal., B* **1995**, *7*, 49. (b) Fujishima, A.; Rao, T. N.; Tryk, D. A. *Electrochim. Acta* **2000**, *45*, 4683.

Table 1. Rate of Incident Photons (R_p^i), Absorption Rate of Incident Photons (R_p^a), CO_2 Generation Rate (R_{CO_2}), and Quantum Efficiencies (QE) for CO_2 Generation Over Different Samples[a]

	Cu(II)−$(Sr_{1-y}Na_y)(Ti_{1-x}Mo_x)O_3$					
	$x = 0$	$x = 0.25\%$	$x = 0.9\%$	$x = 2.0\%$	Cu(II)−TiO_2[b]	Cu(II)−WO_3[b]
R_p^i(quanta/s)	1.30×10^{16}	1.30×10^{16}	1.30×10^{16}	1.30×10^{16}	1.30×10^{16}	1.30×10^{16}
R_p^a(quanta/s)	2.30×10^{14}	6.90×10^{14}	1.00×10^{15}	1.02×10^{15}	3.30×10^{14}	3.91×10^{15}
R_{CO_2} (μmol/h)	0.035	0.043	0.093	0.148	0.029	0.680
QE (%)	15.2	6.1	9.2	14.5	8.8	17.5

[a] Visible light source: wavelength, 400−530 nm; intensity, 1 mW/cm^2. [b] Data from ref 7a.

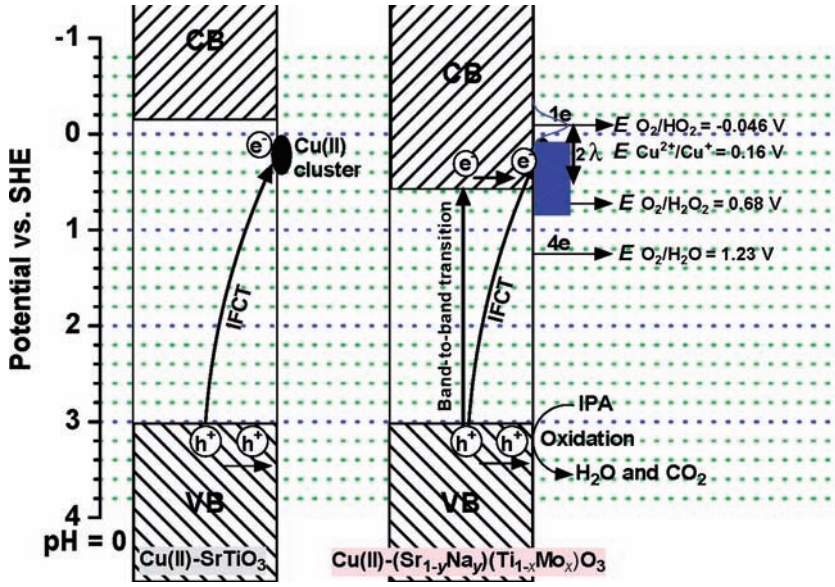

Figure 7. Proposed photocatalysis processes. λ represents the reorganization energy.[7a]

reached a maximum at 0.148 μmol/h, and QE was calculated to be 14.5%. It is worth noting that the activity is much higher than that of Cu(II)−TiO_2 and comparable to that of Cu(II)−WO_3,[7a] suggesting that Cu(II)−$(Sr_{1-y}Na_y)(Ti_{1-x}Mo_x)O_3$ samples are promising visible-light-driven photocatalysts for practical uses.

In order to specify the role of Cu(II) ions, we evaluated the decomposition of IPA over $(Sr_{1-y}Na_y)(Ti_{1-x}Mo_x)O_3$ without Cu(II) ions under UV or visible light irradiation, and the results are shown in Figure 6c. The bare $(Sr_{1-y}Na_y)(Ti_{1-x}Mo_x)O_3$ at $x = 2\%$ without Cu(II) ions was inactive under both UV and visible light irradiation, even though its absorption edge extended to the visible light region. These results reveal that the modification of the doped $SrTiO_3$ with Cu(II) ions is indispensable to achieve its photocatalytic activity. The UV light activities over bare $SrTiO_3$ and Cu(II)−$(Sr_{1-y}Na_y)(Ti_{1-x}Mo_x)O_3$ at $x = 2.0\%$ are shown in Figure 6d in order to discuss its electric band structure. The UV light intensity was calibrated to absorb the same photon numbers as that under visible light irradiation (Figure S7, Supporting Information). Even though the metal ions were doped into Cu(II)−$(Sr_{1-y}Na_y)(Ti_{1-x}Mo_x)O_3$, its UV light activity was better than that of bare $SrTiO_3$. These experiments were performed under the same absorbed photon numbers, indicating that the QE of Cu(II)−$(Sr_{1-y}Na_y)$-$(Ti_{1-x}Mo_x)O_3$ at $x = 2.0\%$ under UV light was about 10%, which was higher than that of bare $SrTiO_3$ under UV light. It is also noteworthy that the photocatalytic activity of Cu(II)−$(Sr_{1-y}Na_y)$-$(Ti_{1-x}Mo_x)O_3$ under UV light irradiation (shown in Figure 6d) was very close to that under visible light irradiation (shown in Figure 6b). To the best of our knowledge, the QE of our materials is the best among the reported perovskite materials or nitrogen-doped TiO_2, and its QE is as high as that reported for very efficient visible light photocatalysts like WO_3. Furthermore, it is also noteworthy that our QE under visible light is the same as that under UV light. This QE trend has never been seen in doped semiconductor photocatalysts such as nitrogen-doped TiO_2.[5] Nitrogen levels in N-doped TiO_2 are isolated above its VB, and its QE under visible light is much lower than that under UV light.[5]

From what has been discussed above, we can draw several important conclusions: (1) The doped sample without Cu(II) modification is inactive for CO_2 generation under UV and visible light irradiation, although lowing the conduction band level can enhance the visible light absorption. (2) After Cu(II) modification, the photocatalytic activity of samples was greatly improved. (3) The QE of Cu(II)−$(Sr_{1-y}Na_y)(Ti_{1-x}Mo_x)O_3$ under visible light irradiation is similar with that under UV light irradiation. (4) The activity of Cu(II)−$(Sr_{1-y}Na_y)(Ti_{1-x}Mo_x)O_3$ under either visible light or UV light irradiation is much better than that of $SrTiO_3$ under UV light irradiation with the same absorbed photon number. (5) The activity of Cu(II)−$(Sr_{1-y}Na_y)$-$(Ti_{1-x}Mo_x)O_3$ can be controlled by tuning the dopants content. Based on the above results, the photocatalytic mechanisms are speculated in Figure 7. Although the absorption edge was extended to the visible light region, the rate of CO_2 generation was negligible over $(Sr_{1-y}Na_y)(Ti_{1-x}Mo_x)O_3$ without Cu^{2+} modification. This can be understood by considering the low potential of photoinduced electrons in the CB. Mo^{6+} as well as Na^+ doping shifted the bottom of the CB more positive than the potential for the single-electron reduction of oxygen ($E =$

−0.064 V vs SHE, pH = 0),[25] resulting in inefficient consumption of photoinduced electrons by oxygen. Once the sample was grafted with Cu(II), the potential of Cu^{2+}/Cu^{+} was about 0.16 V (vs SHE, pH = 0); thus, it can be expected to act as a co-catalyst to reduce oxygen molecules efficiently.[7] Therefore, for Cu(II)−$SrTiO_3$ (at $x = 0$), under visible light irradiation, the holes in the VB resulting from IFCT decomposed IPA, while photoinduced electrons were consumed via an efficient oxygen reduction process with Cu ions, which accounts for the enhanced activity compared to that of bare $SrTiO_3$. For Cu(II)−$SrTiO_3$ doped with Mo^{6+} as well as Na^{+}, by virtue of CB control, in addition to the IFCT process, the electrons in the VB can also be promoted to the CB under visible light irradiation. The photoindued electrons in the CB were further transferred to Cu(II) clusters and drove the oxygen reduction, which retarded the photoindued electron−hole recombination effectively. Consequently, high visible light photocatalytic activity is achieved over Cu(II)−(Sr$_{1-y}$Na$_y$)(Ti$_{1-x}$Mo$_x$)O$_3$ samples as a result of lowering the bottom of the CB and surface Cu(II) modification.

4. Conclusion

In summary, we have developed a novel visible-light-driven photocatalyst based on CB control and surface modification with Cu(II). Our studies show that Mo^{6+} as well as Na^{+} doping in the lattice of $SrTiO_3$ can lower the bottom of the CB and effectively extend the absorption edge to the visible light region. When the bottom of the CB was lowered, Cu(II) modification was indispensable to achieve photocatalytic activity because the potential of the photoinduced electrons in the CB is too low to initiate the single-electron reduction of oxygen. The role of Cu(II) modification has two main positive effects: (i) IFCT for visible light absorption and (ii) co-catalyst for efficient oxygen reduction to consume the photoinduced electrons. Under the same visible light irradiation condition, the activity of Cu(II)−(Sr$_{1-y}$Na$_y$)(Ti$_{1-x}$Mo$_x$)O$_3$ at $x = 2.0\%$ is much higher than that of Cu(II)−$SrTiO_3$. This is because doping with Mo^{6+} as well as Na^{+} increases the light absorption by lowering the bottom of the conduction band. Therefore, high photocatalytic decomposition of IPA over Cu(II)−(Sr$_{1-y}$Na$_y$)(Ti$_{1-x}$Mo$_x$)O$_3$ samples is achieved by utilization of the high oxidation power of holes in the VB in combination with the efficient oxygen reduction via Cu(II). On the basis of this study, possible candidates for visible-light-active materials are largely extended to other materials. That is, some photocatalytically inactive materials, such as low-conduction-band materials or only UV-light-active materials, could become good candidates for efficient visible-light-active photocatalysts on the basis of our new findings. In other words, our work indicates a strategic way to develop new visible-light-active photocatalysts.

Acknowledgment. This work was performed under the management of the Project To Create Photocatalyst Industry for Recycling-Oriented Society, supported by the New Energy and Industrial Technology Development Organization (NEDO) in Japan.

Supporting Information Available: Table S1, composition of the sample derived from ICP and atomic absorption spectrophotometry; Figures S1 and S2, XRD patterns of samples; Figure S3, TEM images of $SrTiO_3$ and Cu(II)−$SrTiO_3$; Figures S4 and S5, full-scale XPS spectra of samples and comparative studies of Mo 3d core-level and Ti 2p core-level spectra of (Sr$_{1-y}$Na$_y$)(Ti$_{1-x}$Mo$_x$)O$_3$ samples with roughly fixed Mo^{6+} content and different Na^{+} contents; Figure S6, (a) comparative study of the UV−visible spectra of samples with roughly fixed Mo^{6+} content and different Na^{+} contents and (b) relationships between $(ah\nu)^{1/2}$ and photon energy of (Sr$_{1-y}$Na$_y$)(Ti$_{1-x}$Mo$_x$)O$_3$ samples; Table S2, specific surface area values of samples; Figure S7, information on the light source for photocatalytic experiments; Figure S8, comparative studies of CO_2 generation over different samples under visible light irradiation; Figure S9, details of the calculations of quantum efficiency. This material is available free of charge via the Internet at http://pubs.acs.org.

JA105846N

(25) Bard, A. J., Parsons, R., Jordan, J., Eds. *Standard Potentials in Aqueous Solution*; Marcel Dekker: New York, 1985.